

This is the accepted version of the following article:

I. Voynarovych, J. Buzek, K. Palka, M. Vlcek, Spectral dependence of photoinduced optical effects in As<sub>40</sub>S<sub>60-x</sub>Se<sub>x</sub> thin films, In Thin Solid Films, Volume 608, 2016, Pages 8-15, ISSN 0040-6090, <https://doi.org/10.1016/j.tsf.2016.04.013>.

This postprint version is available from URI: <http://hdl.handle.net/10195/67592>

Publisher's version is available from

<http://www.sciencedirect.com/science/article/pii/S0040609016300724?via%3Dihub>



This postprint version is licenced under a [Creative Commons Attribution-NonCommercial-NoDerivatives 4.0 International](https://creativecommons.org/licenses/by-nc-nd/4.0/).

# Spectral dependence of photoinduced optical effects in $As_{40}S_{60-x}Se_x$ thin films.

I. Voynarovych<sup>a</sup>, J. Buzek<sup>a</sup>, K. Palka<sup>a,b\*</sup>, M. Vlcek<sup>b</sup>

<sup>a</sup>*Department of General and Inorganic Chemistry, Faculty of Chemical Technology, University of Pardubice, Studentska 95, Pardubice 532 10, Czech Republic*

<sup>b</sup>*Center of Materials and Nanotechnologies, Faculty of Chemical Technology, University of Pardubice, Studentska 95, Pardubice 532 10, Czech Republic*

## Abstract

Spectral dependence of photoinduced structural transformation and related changes of  $E_g^{opt}$ ,  $\alpha$  and  $n$  of thermally evaporated ternary  $As_{40}S_{60-x}Se_x$  thin films have been studied under the exposure to bandgap and super-/sub-bandgap light of LED. The irradiation by bandgap and super-bandgap light with intensity  $0.1 \text{ W/cm}^2$  leads to partial photoinduced polymerization of molecular structural units into continuous network that is characteristic for the bulk glasses with appropriate stoichiometric composition. The efficiency of structural transformation depends on penetration depth of excitation beam. The maximum photosensitivity (i.e. changes of  $E_g^{opt}$ ,  $\alpha$  and  $n$ ) were achieved at the wavelengths  $\sim 100 \text{ nm}$  above the bandgap wavelength for each appropriate composition. Beyond the region of maximal photosensitivity the values of optical parameters and kinetics of photoinduced changes depend on relation between exposed and unexposed sublayer for super-bandgap beams or on absorption coefficient for sub-bandgap light.

Keywords: Ternary As–S–Se chalcogenide glasses, Thin films, Photoinduced effects

\* Corresponding author: Tel.: +420 466 037 408; E-mail address: [Karel.Palka@upce.cz](mailto:Karel.Palka@upce.cz)

## 1. Introduction

The structural flexibility of glass network in amorphous chalcogenide thin films results in plethora of photo-induced changes of optical, structural and surface properties [1, 2]. Thus, such chalcogenide glass (ChG) thin films are promising materials for various applications in integrated optics/photonics such as, photo- and electron resists [3], optical storage and memory devices [4] and in all-optical processing such as waveguides, optics amplifiers, diffraction gratings, microlenses [5–8], ultra-fast optical switches [9], etc. Most applications are based on the well-known photo-induced changes of linear optical constants (i.e.  $\alpha$ ,  $E_g^{opt}$ ,  $n$ ), nonlinear optical constants (i.e.  $\chi(3)$  and  $n_2$ ), thickness of the film ( $\Delta d$ ), phase of the material (i.e. amorphous or crystalline), and their resistance to alkali solvents etc. [2, 10]. Generally, photoinduced structural changes on the freshly deposited thin films are almost completely irreversible. Mechanism of these photoinduced structural transformations depends mainly on absorption coefficient and penetration depth of photons with appropriate energy, efficiency of electron-hole excitation, displacement of atoms and/or switching bonds due to creation or amplification of phonons by excited electrons [1]. Thus, the degree of photoinduced structural transformation depends mainly on parameters of exposure beam (intensity, energy, polarization can also play an important role) as well as on the thin films properties (composition, network structure and prehistory). It is obvious and well known that noticeable photoinduced structural transformation of as-evaporated thin films network can be obtained by irradiation of bandgap and super-bandgap light with moderate intensity or sub-bandgap light with high intensity [3]. In most of the previous studies, the exposure by cw Ar<sup>+</sup>, He–Ne or He–Cd lasers ( $\lambda=514.5$ , 632.8 and 441.6 nm respectively) were used to investigate changes in optical/structural/surface properties of ChG thin films [11–13]. In details the spectral dependence of photoinduced structural transformation were investigated mainly for binary  $As_2S_3$  [14] and  $As_{50}Se_{50}$  [15] thin films.

Ternary amorphous  $As_{40}S_{60-x}Se_x$  ( $x=0, 10, 20, 30, 40, 50, 60$ ) as-evaporated thin films were in focus of our interest in present study. The spectral dependences of photoinduced non-reversible structural transformation and related changes of optical properties were investigated under irradiation by relatively narrow-band light beams that cover energy region from super- to sub-bandgap for each particular composition. The observed effects were compared with those changes induced by broad band exposure.

## 2. Experimental

Bulk  $As_{40}S_{60-x}Se_x$  glasses were prepared from pure 99.999% elements by conventional melt quenching technique. The starting materials were weighed and sealed in quartz ampoules in the vacuum. The sealed ampoules were heated in furnace at 500 °C over 24 h, and after that the temperature was raised up to 850 °C for 10 h. In order to ensure the homogenization of molten glasses, the ampoules were frequently rocked at maximum temperature. The quenching was done into cold water. Thin films of synthesized glasses were prepared using thermal evaporation technique on cleaned glass substrates at room temperature (Tesla Corporation, model UP-858) at pressure of  $\sim 2 \times 10^{-4}$  Pa ( $10^{-6}$  Torr), and with evaporation rate 1–2 nm/sec. Thickness of the thin films was in the range 200–1000 nm. During evaporation, the substrates were kept rotating by planetary rotation system, so that the thickness uniformity of the films was maintained. After evaporation thin films were stored inside the deposition chamber for  $\sim 24$  h to achieve the metastable equilibrium.

As-deposited thin films were exposed by halogen lamp with red cut-off filter near 700 nm and LED diodes Roither Lasertechnik (Austria) emitting beams with maximum outputs at wavelengths 375, 405, 450, 525, 630, 690, 740 and 790 nm and intensity  $\sim 100$  mW/cm<sup>2</sup>, with exposure times up to 60 minutes for each sample. Transmission spectra of thin films during

the exposure were measured *ex-situ* on custom-made setup equipped by fiber spectrometer EPP2000 (StellarNet Inc.) in times from 30 second to 60 minutes. From these optical transmission spectra the wavelengths  $\lambda_t$  at  $T=10\%$  were deducted as a functions of exposure time for particular exposure wavelengths. Time dependences were also empirically fitted by the known stretched exponential function [16]:

$$y = A \left[ 1 - \exp \left\{ - \left( \frac{t}{\tau} \right)^\beta \right\} \right] \quad (1),$$

where  $A$  is a constant (equal to the total change at  $t \rightarrow \infty$ ,  $\Delta\lambda_{max}$  in our case),  $\tau$  and  $\beta$  are the effective response time and the dispersion parameter, respectively,  $t$  is time, and  $y$  is the difference between wavelengths  $\lambda$  ( $T=10\%$ ) in exposed and as-prepared thin film's spectra at time  $t$ . All exposures were done in air. The optical transmissions of unexposed and fully exposed  $As_{40}S_{60-x}Se_x$  thin films were measured by double beam UV/VIS/NIR computerized spectrophotometer (Shimadzu, Model UV-3600) in wavelength range of 300–3000 nm. Raman spectra were measured using FTIR spectrometer IFS 55 (Bruker) with Raman spectroscopy module FRA 106 working with excitation source Nd:YAG laser (1064 nm). An atomic force microscope (NT-MDT, NEXT) was used to investigate the morphology of the surface of the exposed thin films.

### 3. Results

Transmittance spectra of as-deposited amorphous  $As_{40}S_{60-x}Se_x$  thin films are plotted in Fig. 1, showing a clear red shift of absorption edge with increasing  $Se$  concentration. For comparison the spectral characteristics of all used LEDs are given in the Fig. 1 too. The *FWHM* of used LEDs are in range 15–45 nm, and for further discussion we will use term “narrow band” to distinguish spectral band of LED with the mentioned above *FWHM* from monochromatic light of laser. The difference  $\Delta\lambda$  between wavelengths  $\lambda_t$  deducted at  $T=10\%$  from exposed at

time  $t$  and as-prepared thin film's transmission spectra were calculated. Fig. 2 shows an example of time dependences of  $\Delta\lambda$  for  $As_{40}S_{30}Se_{30}$  thin film and particular exposure wavelengths. From the dependences  $\Delta\lambda=f(t)$  the largest shifts  $\Delta\lambda_{max}$  between as-prepared and fully exposed thin film were deduced. The dependence of parameter  $\Delta\lambda_{max}$  on composition  $x$  of  $As_{40}S_{60-x}Se_x$  for appropriate LEDs wavelengths and normalized dependence of  $\Delta\lambda_{max}$  on relative wavelength ( $\lambda_{LED} - \lambda(E_g^{opt})$ ) for 1  $\mu\text{m}$  thick thin films were drawn (Figs. 3a and b respectively). In the Fig. 3c the normalized functions of maximum shifts  $\Delta\lambda_{max}=f(\lambda_{LED} - \lambda(E_g^{opt}))$  were drawn for different thicknesses and specific compositions of investigated thin films. From these dependences the LEDs for exposure were chosen that relate to super-, sub-, and bandgap light. As a source of super-bandgap light the diode with  $\lambda_{LED}=405$  nm was chosen for all compositions due to relatively smaller surface damage contrary to the LED with  $\lambda_{max}=375$  nm. The LEDs from region of maximum sensitivity and energy below bandgap were chosen as the emitters of bandgap and sub-bandgap light, respectively (listed in Table 1). Parameters of stretched exponential function (1) describing kinetics of the photoinduced changes are presented in Table 2.

Raman spectra of the bulk glasses, thermally evaporated films and exposed films of investigated compositions  $As_{40}S_{60-x}Se_x$  are presented in Figs. 4 and 5. The most intense bands in the Raman spectra of these ternary compositions are located around 225 and 345  $\text{cm}^{-1}$ , which is near the band maxima positions in the spectra of the extreme compositions ( $As_{40}S_{60}$  and  $As_{40}Se_{60}$ ). A good correlation is observed in the spectral position and form of the most intense bands of the thermally deposited film and the corresponding bulk glass. Beside the main bands in the spectra of the films additional weak bands appeared, i.e., the main broad bands (regions 220–260 and 320–380  $\text{cm}^{-1}$ ) are structured, and some additional weaker bands (mainly in the region 125–200  $\text{cm}^{-1}$ ) exist in the Raman spectra of virgin films. These differences between the spectra of as-deposited thin films and bulk glasses become more

significant as the  $S$  content in the  $As_{40}S_{60-x}Se_x$  thin films increases – differences are not so notable in the case of exposed samples.

The optical transmission spectra  $T(\lambda)$  taken at normal incidence, of as-evaporated and exposed amorphous  $As_{40}S_{60-x}Se_x$  thin films have been used for calculation of optical parameters ( $n(\lambda)$ ,  $\alpha(h\nu)$ ,  $E_g^{opt}$ ) by well-known method proposed by Swanepoel [17]. The results of calculations are listed in Table 1.

Spectral dependencies of refractive index  $n(\lambda)$  for the as-evaporated thin films and thin films exposed by broadband halogen lamp and LEDs of specified wavelengths are plotted in Fig. 6. The dispersion of the refractive index has been analyzed on the basis of the Wemple–DiDomenico (WDD) model [18, 19], which uses the single-oscillator equation

$$n^2(h\nu) = 1 + \frac{E_o E_d}{E_o^2 - (h\nu)^2} \quad (2)$$

where  $E_o$  is the single-oscillator energy and  $E_d$  the dispersion energy or single-oscillator strength.  $E_o$  is considered as an average energy gap and, to a good approximation, it varies in proportion to the Tauc gap,  $E_g^{opt}$ :  $E_o \approx 2E_g^{opt}$  [20]. By plotting  $(n^2 - 1)^{-1}$  against  $h\nu^2$  and fitting a straight line,  $E_o$  and  $E_d$  can be directly determined from the slope  $(E_o E_d)^{-1}$ , and the intercept  $E_o/E_d$ , on the vertical axis. The WDD model is only valid in the transmission region, where the absorption coefficient of the chalcogenide film takes values  $\alpha \approx 0$ . Therefore, due to optical absorption, the experimental energy variation in the refractive index deviates from that given by Eq. (2) when the photon energy approaches  $E_g^{opt}$ . The values of the parameters  $E_o$  and  $E_d$ , as well as the value of the refractive index at  $h\nu \rightarrow 0$  (extrapolating the WDD optical dispersion relationship towards the infrared spectral region),  $n(0)$  with accuracies  $\approx 1\%$  for the as-evaporated and exposed amorphous  $As_{40}S_{60-x}Se_x$  thin films, are listed in Table 1.

Analysis of the high-absorption region ( $\alpha \approx 10^4 \text{ cm}^{-1}$ ) has been carried out by well-known quadratic equation – often called the Tauc law [21]. The values of  $E_g^{opt}$  for the as-

evaporated and exposed amorphous  $As_{40}S_{60-x}Se_x$  films have been derived by plotting  $(\alpha h\nu)^{1/2}$  versus  $h\nu$  as displayed in Fig. 7, and are listed in Table 1.

Compositional dependencies of optical band gap energy ( $E_g^{opt}$ ) as well as refractive index of as-evaporated and exposed thin films are plotted in Fig. 8, showing a clear decreasing of  $E_g^{opt}$  and increasing refractive index  $n$  with increasing  $Se$  content as well as decreasing of  $E_g^{opt}$  and increasing of refractive index after exposure for each particular composition.

An AFM images of  $As_{40}S_{50}Se_{10}$  thin film surface exposed by UV LED with  $\lambda=375$  nm and 405 nm are shown in Fig. 9. The AFM investigation shows a growth of crystallites with triangle shape and size of 1–2  $\mu\text{m}$  on exposed by UV LED (with  $\lambda=375$  nm) surface, and much smaller surface structures on exposed by LED with  $\lambda=405$  nm.

#### 4. Discussion

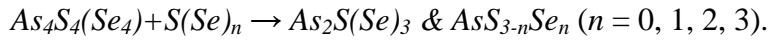
It is well known that change of optical parameters of as-evaporated chalcogenide thin films with exposure is apparently connected with photoinduced irreversible changes of structure [1, 2]. Raman spectroscopy method is widely used to study photostructural transformation in amorphous chalcogenide glasses as well as their thin films. The Raman spectra of thermally evaporated thin films and bulk glasses of stoichiometric  $As_{40}S_{60}$  or  $As_{40}Se_{60}$  compositions (see Fig. 4), shows the dominant bands at  $345\text{ cm}^{-1}$  and  $228\text{ cm}^{-1}$  respectively, which corresponds to the presence of  $AsS_{3/2}$  and  $AsSe_{3/2}$  pyramids. The shoulders at  $312$  and  $380\text{ cm}^{-1}$  are assigned to the interaction between the  $AsS_{3/2}$  pyramids. In case of ternary  $As-S-Se$  bulk glasses, the replacement of chalcogens of one type by chalcogens of another type takes place, and thus the structure of the as-evaporated  $As_{40}S_{60-x}Se_x$  layers also should contain mixed  $AsS_{3-n}Se_n$  ( $n = 0, 1, 2, 3$ ) pyramidal structural units [22]. The Raman spectra of bulk glasses



and thin films that contain this mixed structural units, according to [22, 23], do not exhibit new bands in comparison with stoichiometric  $As_{40}S_{60}$  or  $As_{40}Se_{60}$  glasses. Due to thermal dissociation of bulk glass the structure of freshly prepared thin films of  $As-S-Se$  ternary composition contain some of the binary molecular species, e.g.,  $As_4S_4$  ( $As_4Se_4$ ),  $As_4S_3$  ( $As_4Se_3$ ), significant number of mixed ternary molecular species such as  $As_4S(Se)_4$ ,  $As_4S(Se)_3$ , as well as  $S_8$  rings,  $S_n(Se_n)$  chains and  $As_4$  molecular fragments [23, 24] which are dissolved in glass network as molecular or nano-sized particles. Because of their molecular nature, the Raman spectra of freshly evaporated thin films consist of number of narrow bands [25, 26]. The intense and narrow bands in Raman spectra of thin films (see Fig. 4) between  $135\text{ cm}^{-1}$  and  $234\text{ cm}^{-1}$  and also at  $363\text{ cm}^{-1}$  are related to vibration of the above mentioned molecular units containing ‘wrong’ homopolar  $As-As$  bonds. The narrow band near  $254\text{ cm}^{-1}$  can be assigned to  $Se_8$  rings vibrations, the band near  $240\text{ cm}^{-1}$  is formed by overlapping of bands assigned to  $Se_n$  chains and  $As_4(S)Se_3$  molecules vibrations [27]. The two bands at  $495$  and  $474\text{ cm}^{-1}$  are related  $S-S$  bond vibration of  $S_n$  chains and  $S_8$  rings, respectively.

Comparison between Raman spectra of  $As_{40}S_{30}Se_{30}$  bulk glass, as-deposited thin films ( $d = 1\text{ }\mu\text{m}$ ) and thin films ( $d = 1\text{ }\mu\text{m}$ ) exposed by wide band and with narrow band light of different wavelengths is shown on Fig. 5. Raman spectra of thin films exposed by halogen lamp (curve 2, Fig. 5) as well as by band gap LED (curve 3, Fig. 5) are very close to that of the Raman spectra of bulk glass (curve 1, Fig. 5). It confirms that significant structural changes appear at energies equal or slightly higher than is the bandgap energy. As can be seen from Figs. 4 and 5, the exposure of as-deposited  $As-S-Se$  films causes significant decrease in intensity of narrow bands associated with ‘wrong’  $As-As$  bonds in region  $100-234\text{ cm}^{-1}$ ;  $S-S$  bonds at  $474$  and  $495\text{ cm}^{-1}$ ;  $Se-Se$  bonds at  $255, 270\text{ cm}^{-1}$  and broad band at  $440-480\text{ cm}^{-1}$ . The decreasing of ‘wrong’ bonds content indicate the transformation of above mentioned molecular species to the binary  $AsS_{3/2}$  and  $AsSe_{3/2}$  as well as mixed  $AsS_{3-n}Se_n$  ( $n =$

0, 1, 2, 3) pyramidal structural units of chalcogenide glass network, i.e. the photoinduced chemical reaction [1, 2]. One of the main such polymerization scheme is:



Exposure by super-bandgap LED (curve 4, Fig. 5) of 1  $\mu\text{m}$  thick thin film modifies the structure less effectively. The explanation of such dependences is rather related to the energy dependence of light penetration depth. If penetration depth of wavelength of particular LED is sufficient to cover the whole thickness of the thin film, the structural transformation will be similar. This is proved by Raman spectra of 200 nm thick film (see curve 4', Fig. 5) exposed with super-bandgap LED with wavelength  $\lambda_{LED}=405$  nm.

Irradiation by LED with sub-bandgap wavelength does not cause significant decrease in intensity of narrow bands in region  $100\text{--}234$   $\text{cm}^{-1}$ , associated with 'wrong' As–As bonds of  $As_4S(Se)_4$ ,  $As_4S(Se)_3$  molecular cages. The decreasing intensity of narrow band at 220 and 254  $\text{cm}^{-1}$  (curve 5, Fig. 5) indicates that the transformation is connected mainly with decrease of Se–Se bonds associated with  $Se_8$  rings and  $Se_n$  chains.

The photoinduced polymerization of as-evaporated thin films causes change of optical properties, i.e. absorption spectra  $\alpha(h\nu)$  and refraction coefficient  $n(\lambda)$ . The spectral and compositional dependence of the refractive index for the as-prepared, exposed by halogen lamp and multiple LEDs amorphous  $As_{40}S_{60-x}Se_x$  films are shown on Figs. 6 and 8, respectively. Increase in the values of the refractive index is observed with increasing Se concentration as well as with irradiation by LED with wavelength close to band gap energy and especially in case of irradiation by halogen lamp, over the whole spectral region under study. It is well known that refractive index could be explained on the basis of the Lorentz–Lorenz relationship [28]:

$$\frac{n^2-1}{n^2+2} = \frac{1}{3\epsilon_0} \sum_j N_j \alpha_{p,j} \quad (3)$$

where  $\epsilon_0$  is the vacuum permittivity and  $N_j$  the number of polarizable units of type  $j$  per volume unit, with polarizability  $\alpha_{p,j}$ . Thus, the increase of refractive index with increasing Se content connected with larger polarizability  $\alpha_{p,j}$  of Se atoms (atomic radius of Se atoms is larger in comparison with S atoms). The structural densification during the above mentioned photoinduced polymerization process increases the number of polarizable units  $N_j$  per volume, that accordingly, leads to increasing in the refractive index of exposed thin films.

Decrease in the Tauc gap ( $E_g^{opt}$ ) that lead to red shift of the optical absorption edge has been found with increasing Se content (see Figs. 7 and 8) as well as after irradiation by wide band and LED's sub-, super-, and bandgap beams. The maximal values for red shift of Tauc band gap energy of as-evaporated thin films ( $\Delta E_g^{opt}$ ) were achieved in range 40–60 meV after irradiation by wide band beam and narrow band gap LEDs beam for all  $As_{40}S_{60-x}Se_x$  ternary compositions (see Fig. 8 and Table 1). Also a decrease in single oscillator energy  $E_o$  from Wemple–DiDomenico model has been found (see Table 1), as expected from the relation  $E_o \approx 2E_g^{opt}$ . The compositional dependence could be explained according to the previously mentioned relationship by Tanaka [20]. The higher bonding energy of As–S bonds compared with that of As–Se bonds, plausibly explains the compositionally dependent decreasing found in both optical parameters. The decrease of Tauc gap  $E_g^{opt}$  after irradiation is consistent, as it was shown by Raman spectroscopy, with significant decrease in concentration of „wrong“ As–As homopolar bonds (for instance in the  $As_4S(Se)_4$ , and  $As_4S(Se)_3$  species) leading to an also significant increase in the concentration of heteropolar bonds of the type As–S and As–Se, with higher bonding energies than the homopolar ones.

As shown in Fig. 2, the maximum value of red shift is noticed at broadband exposition by halogen lamp, which becomes more significant as the Se content in the  $As_{40}S_{60-x}Se_x$  samples increases. In the case of exposure to LED light the values of the red shift strongly depend on glass composition and wavelength of the LED band maximum. The normalized

dependence of  $\Delta\lambda_{max}$  on relative wavelength  $(\lambda(E_g^{opt})-\lambda_{LED})$  (Fig. 3b) drawn for 1  $\mu\text{m}$  thick thin films gives evidence that the most significant shifts (with values higher than  $0.8\Delta\lambda_{max}$ ) are caused by exposure to the beams with wavelengths that lie up to 100 nm in super-bandgap region. On the contrary the significantly smaller photodarkening takes place with exposures by sub-bandgap beams and further than  $\sim 100$  nm super-bandgap beams. At the same time the  $\Delta\lambda_{max}$  for  $As_2Se_3$  and ternary compositions with high content of *Se* is higher in further than 100 nm super-bandgap region as well as in sub-bandgap region (see Fig. 3b). Decreasing thicknesses of thin films down to 400 nm, 250 nm and even up to 200 nm (curve 1–3, Fig. 3c, respectively) significantly increases the region of maximum photosensitivity up to 300 nm in super-bandgap region.

According to theory of light interaction with amorphous chalcogenide glasses [1, 2], an efficiency of photoinduced structural transformation depends on few parameters: (1) efficiency of electron-hole excitation, which mainly depends on correlation between distribution of density of localized states near conduction and the valence band and energy of excitation beam; (2) distribution of molecules or structural units able to transformation across the thin film thickness (i.e. homogeneity of thin film) and (3) distribution of light intensity across the thin film thickness (i.e. penetration depth). Let us consider influence of each parameter on efficiency of photoinduced irreversible structural transformation of ternary chalcogenide  $As_{40}S_{60-x}Se_x$  thin films.

The structure of as deposited ternary thin films with high content of *Se*, as was shown above by Raman spectroscopy, consist of randomly spread molecular species such as  $As_4S(Se)_4$ ,  $As_4S(Se)_3$  molecular cages,  $Se_8$  rings and  $Se_n$  chains over the structural network. These molecular cages and especially selenide rings and chains create deep localized states in bandgap which result in broader distribution density of localized states. The broader

distribution of localized states is responsible for wider region of photoinduced structural transformation of  $As_2Se_3$  and ternary composition with high  $Se$  content (see Fig. 3b).

Due to different partial vapor pressure of each glass component during the vacuum thermal evaporation, the homogeneity of chalcogenide thin films with different composition is under permanent focus of interest. The homogeneity of ternary  $As_{40}S_{60-x}Se_x$  with  $x=0, 30, 60$  were investigated in detail in reference [29]. In this paper investigation of refractive index of thin films with different thickness ranging from  $\lambda/20$  to  $2\lambda$  ( $\lambda=632.8$  nm) has been done by ellipsometry. Authors of [29] found that thin films with thickness  $d>50$ nm have constant refractive index, e.g. ternary  $As_{40}S_{60-x}Se_x$  thin films prepared by vacuum thermal evaporation are homogeneous.

The intensity distribution of excitation beam can be calculated from absorption coefficient according to Lambert–Beer law:  $I = I_0 e^{(-\alpha d)}$ . In Fig. 10 an example of intensity distribution across film thickness for LEDs with different peak maxima wavelengths and  $As_{40}S_{30}Se_{30}$  thin film is shown. As can be seen, the super-bandgap beams of emitting diodes penetrate only several tens or hundreds of nanometers of thin film surface. Taking into account that for chalcogenide glass thin films exposed by light with moderate intensity, the reciprocal law is roughly correct [1], the induced photostructural changes occurs mainly in these depths, with appropriate much smaller changes in entire thin film. Because the exponential decreasing of incident beam intensity takes place, decreasing thickness of thin film significantly increases the region of maximum photoinduced structural transformation (see curve 1–3, Fig. 3).

The absorption of excitation beam in penetration depth ( $d_{pd}$ ) influences not only values of photoinduced optical properties, but also kinetics of structural transformation. In [16, 30, 31] was shown, that when the film thickness  $d$  is smaller than  $1/e$ , (i.e.,  $d < d_{pd}$ ), the dispersion parameter of stretched exponential function  $\beta$  (equation 1) is close or equal to 1,

indicating that the dynamics is presented by an exponential function. Under the condition of  $d > d_{pd}$ , the dynamic response becomes dispersive in nature and hence  $\beta$  became smaller of unity. The results of analysis of darkening kinetics according to equation 1 for some ternary thin films are presented in Table 2.

According to these data we can conclude, that the spectral region of maximum efficiency of photoinduced structural transformation, with the most effective kinetic properties for ternary As–S–Se composition increases with increasing of Se content and with decreasing of thin film thickness.

We found that after 60 minutes exposures partial surface destruction of samples took place for all used diodes. In case of UV LED with  $\lambda=375$  nm exposed surface exhibited strong scattering of light, visible even by eye. AFM investigation of  $As_{40}S_{50}Se_{10}$  thin film surfaces exposed by UV LED with  $\lambda=375$  nm shows a growth of crystallites with triangle shape that is typical for arsenic trioxide ( $As_2O_3$ ) and size of 1–2  $\mu\text{m}$ , as can be seen on Fig. 9a. Irradiation by LED with peak wavelength 405 nm leads to creation a much smaller surface structures (see Fig. 9b). In both cases creation of crystallites on surface of thin film can be caused by partial oxidation of As–As bonds during long exposures which is in good agreement with data given in [32, 33]. As was shown in [14], the super-bandgap light can form S-rich layer on the surface of chalcogenide thin films.

## 5. Conclusions

Exposure by multiple wavelength beams with super-bandgap and bandgap energy of thermally deposited ternary  $As_{40}S_{60-x}Se_x$  thin films ( $x = 0, 10, 20, 30, 40, 50$  and  $60$  at.%) significantly changes their network structure and optical properties ( $E_g^{opt}$ ,  $\alpha$  and  $n$ ). The photoinduced structural transformations are directed to non-reversible reduction of molecular fragments that contain “wrong” homopolar bonds and formation of continuous bulk-like

network. The range of maximum efficiency of photoinduced structural transformation weakly increases with increasing *Se* content in thin films composition and significantly increases up to 300 nm above the wavelength which corresponds to the bandgap energy for appropriate composition with decreasing thin film thickness. Thus for thinner films the region of photosensitivity is broader than for thicker thin films of the same composition.

### **Acknowledgements**

This work was supported by the grant Development of Research Teams at the University of Pardubice CZ.1.07/2.3.00/30.0058 from the Czech Ministry of Education, Youth and Sports. The authors also thank to project CZ.1.05/4.1.00/11.0251 Center of Materials and Nanotechnologies co-financed by the European Fund of the Regional Development and the state budget of the Czech Republic.

### **References**

- [1] A. V. Kolobov, Photo-induced metastability in amorphous semiconductors. Wiley-VCH, 2003.
- [2] K. Tanaka, K. Shimakawa, Amorphous Chalcogenide Semiconductors and Related Materials. Springer, 2011.
- [3] A. Kovalski, M. Vlcek, J. Cech, W.R. Heffner, C.M. Waits, M. Dubey, H. Jain, Chalcogenide glass e-beam and photoresists for ultrathin grayscale patterning, J Mikro/Nanolithogr. MEMS MOEMS 8 (2009) 043012–1–11.
- [4] M. Wutting, N. Yamada, Phase change materials for rewriteable data storage, Nature Mater. 6 (2007) 824–832.

- [5] A. Andriesh, Chalcogenide glasses as multifunctional photonic materials, *J. Optoelectron. and Adv. Mat.* 7 (2005) 2931–2939.
- [6] T. Wagner, P. J. S. Ewen, Photo-induced dissolution effect in  $Ag/As_{33}S_{67}$  multilayer structures and its potential application, *J. Non-Cryst. Solids* 266–269 (2000) 979–984.
- [7] G. Beadie, W. S. Rabinovich, J. Sanghera, I. Aggarwal, Fabrication of microlenses in bulk chalcogenide glass, *Opt. Commun.* 152 (1998) 215–220.
- [8] A.V. Stronski, M. Vlcek, A. Sklenar, P.E. Shepeljavi, S.A. Kostyukevich, T. Wagner, Application of  $As_{40}S_{60-x}Se_x$  layers for high-efficiency grating production, *J. Non-Cryst. Solids* 266–269 (2000) 973–978.
- [9] K. Ogusu, J. Yamasaki, S. Maeda, M. Kitao, M. Minakata, Linear and nonlinear optical properties of  $Ag-As-Se$  chalcogenide glasses for all-optical switching, *Opt. Lett.* 29 (2004) 265–267.
- [10] M. Vlcek, S. Schroeter, J. Cech, T. Wagner, T. Glaser, Selective etching of chalcogenides and its application for fabrication of diffractive optical elements, *J. Non-Cryst. Solids* 326&327 (2003) 515–518.
- [11] A. Arsh, M. Klebanov, V. Lyubin, L. Shapiro, A. Feigel, M. Veinger, B. Sfez, Glassy  $mAs_2S_3 \cdot nAs_2Se_3$  photoresist films for interference laser lithography, *Opt. Mat.* 26 (2004) 301–304.
- [12] J. Teteris, M. Reinfelde, Holographic recording in amorphous chalcogenide semiconductor thin films, *J. Non-Cryst. Solids* 326&327 (2003) 494–499.
- [13] K. Antoine, H. Jain, M. Vlcek, Optical spectroscopy of  $a-As_2Se_3$  under in situ laser irradiation, *J. Non-Cryst. Solids* 352 (2006) 595–600.
- [14] A. Kovalskiy, M. Vlcek, K. Palka, R. Golovchak, H. Jain, Wavelength dependence of photostructural transformation in  $As_2S_3$  thin films, *Phys. Procedia* 44 (2013) 75–81.



- [15] K. Palka, M. Vlcek, J. Mistrik, Study of  $As_{50}Se_{50}$  thin film photodarkening induced by multiple wavelength beams, *J. Optoelectron. and Adv. Mat.* 13 (2011) 1510–1513.
- [16] K. Shimakawa, N. Nakagawa, T. Itoh, The origin of stretched exponential function in dynamic response of photodarkening in amorphous chalcogenides, *Appl. Phys. Lett.* 95 (2009) 051908.
- [17] R. Swanepoel, Determination of the thickness and optical constants of amorphous silicon, *J. Phys. E: Sci. Instrum.* 16 (1983) 1214–1223.
- [18] S. H. Wemple, M. DiDomenico, Behavior of the electronic dielectric constant in covalent and ionic materials, *Phys. Rev. B* 3 (1971) 1338–1351.
- [19] S. H. Wemple, Refractive-index behavior of amorphous semiconductors and glasses, *Phys. Rev. B* 7 (1973) 3767–3777.
- [20] K. Tanaka, Optical properties and photoinduced changes in amorphous  $As-S$  films, *Thin Solid Films* 66 (1980) 271–276.
- [21] J. Tauc, Optical properties of amorphous semiconductors in, J. Tauc (Ed.), *Amorphous and Liquid Semiconductors*, Plenum, London & New York, 1974, pp. 159-220.
- [22] J.A. Freitas, U. Strom, D.J. Treacy, Raman scattering of the mixed chalcogenide glass system  $As_2S_xSe_{3-x}$ , *J. Non-Cryst. Solids* 59&60 (1983) 875–878.
- [23] E.J. Felty, G. Lukovsky, M.B. Myers, Optical properties of the mixed amorphous system  $As_2S_xSe_{3-x}$ , *Solid State Commun.* 5 (1967) 555–558.
- [24] P. Nemeč, J. Jedelský, M. Frumar, M. Stabl, M. Vlcek, Structure, thermally and optically induced effects in amorphous  $As_2Se_3$  films prepared by pulsed laser deposition, *J. Phys. and Chem. Solids* 65 (2004) 1253–1258.
- [25] V. Kovanda, M. Vlcek, H. Jain, Structure of  $As-Se$  and  $As-P-Se$  glasses studied by Raman spectroscopy, *J. Non-Cryst. Solids* 326&327 (2003) 88–92.

- [26] A. Sklenar, M. Vlcek, P. Bezdicka, in Proceedings of the Fifth ESG Conference „Glass science and technology for 21st century“, A. Helebrant, M. Maryska and S. Kasa (Eds.), Czech Glass Soc, Prague, 1999, C1-99.
- [27] M. Vlcek, A.V. Stronski, A. Sklenar, T. Wagner, S.O. Kasap, Structure and imaging properties of  $As_{40}S_{60-x}Se_x$  glasses, *J. Non-Cryst. Solids* 266–269 (2000) 964–968.
- [28] S.R. Elliott, *The Physics and Chemistry of Solids*, Wiley, Chichester, 2000.
- [29] R. Todorov, J. Tasseva, V. Lozanova, A. Lalova, Tz. Iliev, A. Paneva, Ellipsometric characterization of thin films from multicomponent chalcogenide glasses for application in modern optical devices, *Adv. Cond. Mat. Phys.* 2013 (2013) 1–11.
- [30] V.O. Balitska, M.S. Iovu, O.I. Shpotyuk, Stretched exponential parameterization of in-situ photodarkening kinetics in amorphous As–Se films, *J. Non-Cryst. Solids* 377 (2013) 182–185
- [31] S.H.M. Shieh, W.C. LaCourse, Aging and sub- $T_g$  relaxation in arsenic selenide glass fibers, *Mater. Chem. Phys.* 35 (1993) 160–167.
- [32] J. T. Bloking, S. Krishnaswami, H. Jain, M. Vlcek, R.P. Vinci, Photoinduced changes in the surface morphology of  $As_{50}Se_{50}$  chalcogenide glass films, *Opt. Mater.* 17 (2001) 453–458.
- [33] R.J. Nemanich, G.A.N. Connel, T.M. Hayers, R.A. Street, Thermally induced effects in evaporated chalcogenide films. I. Structure, *Phys. Rev. B* 18 (1978) 6900–6914.

Fig. 1. Characteristics of the diodes used for exposure and transmission spectra of as-prepared  $As_{40}S_{x-60}Se_x$  thin films (film thickness  $d \sim 1000\text{nm}$ ).

Fig. 2. Dependences of  $\Delta\lambda=f(t)$  ( $T=10\%$ ) for particular exposure wavelengths ( $As_{40}S_{30}Se_{30}$ ). The line is fitted using eq.(1).

Fig. 3. Dependence of  $\Delta\lambda_{max}$  on composition of  $As_{40}S_{60-x}Se_x$  (a) and normalized dependence of  $\Delta\lambda_{max}$  on relative wavelength according to band gap energy of each composition for 1  $\mu\text{m}$  thick thin films (b) and for lower film thicknesses (c). The line through the data points is to guide the eye.

Fig. 4. Raman spectra of bulk (dashed line), as-deposited (solid line) and exposed by halogen lamp thin films (dotted line) of  $As_{40}S_{x-60}Se_x$  samples.

Fig. 5. Raman spectra of bulk  $As_{40}S_{30}Se_{30}$  (1) and as-deposited (6), exposed by halogen lamp (2) and band gap ( $\lambda_{LED}=525$  nm) (3), sub-band gap ( $\lambda_{LED}=690$  nm) (5) and super-band gap ( $\lambda_{LED}=405$  nm) LED (4, 4')  $As_{40}S_{30}Se_{30}$  thin film samples.

Fig. 6. Refractive index dispersion of the amorphous  $As_{40}S_{60-x}Se_x$  thin films obtained from their transmission spectra. Curves have been drawn according to Eq. (2)

Fig. 7. Determination of the optical gaps in terms of Tauc's law, as linear extrapolation of the absorption data.

Fig. 8. Dependence of band gap energy ( $E_g^{opt}$ ) and refractive index of as-deposited and exposed amorphous  $As_{40}S_{60-x}Se_x$  thin films on composition  $x$ . The line through the data points is to guide the eye.

Fig. 9. AFM images of  $As_{40}S_{50}Se_{10}$  thin film surfaces after exposition by LEDs with peak wavelength 375 nm (a) and 405 nm (b) for 60 min.

Fig. 10. Spectral dependence of the penetration depth of LEDs beam in  $As_{40}S_{30}Se_{30}$  thin film.

Table 1

Changes of optical parameters under wide-band and narrow-band irradiations of amorphous

$As_{40}S_{60-x}Se_x$  films.

x, at.%	status	$n(0)$	$\Delta n(0)$	$E_g^{opt},$ eV	$\Delta E_g^{opt},$ eV	$E_0, eV$	$E_d, eV$
0	as-deposited	2.33		2.39		5.03	22.27
	halogen lamp	2.39	0.06	2.36	0.04	4.89	23.08
	$\lambda_{overBG}^{LED} = 405nm$	2.36	0.03	2.37	0.02	5.02	22.94
	$\lambda_{BG}^{LED} = 450nm$	2.39	0.06	2.35	0.04	4.94	23.17
	$\lambda_{subBG}^{LED} = 570nm$	2.38	0.05	2.38	0.01	4.98	23.16
10	as-deposited	2.37		2.25		4.722	21.73
	halogen lamp	2.45	0.08	2.19	0.06	4.621	23.07
	$\lambda_{overBG}^{LED} = 405nm$	2.42	0.05	2.22	0.03	4.415	21.40
	$\lambda_{BG}^{LED} = 525nm$	2.44	0.07	2.21	0.047	4.486	22.19
	$\lambda_{subBG}^{LED} = 630nm$	2.41	0.04	2.24	0.01	4.55	21.78
20	as-deposited	2.41		2.14		4.69	22.54
	halogen lamp	2.50	0.09	2.09	0.05	4.42	23.12
	$\lambda_{overBG}^{LED} = 405nm$	2.43	0.02	2.12	0.02	4.42	21.76
	$\lambda_{BG}^{LED} = 525nm$	2.49	0.08	2.095	0.05	4.43	22.95
	$\lambda_{subBG}^{LED} = 690nm$	2.44	0.03	2.14	0.004	4.66	23.10

30	as-deposited	2.49		2.04		4.30	22.38
	halogen lamp	2.56	0.07	1.99	0.05	4.25	23.49
	$\lambda_{overBG}^{LED} = 405nm$	2.495	0.005	2.02	0.02	4.44	23.17
	$\lambda_{BG}^{LED} = 525nm$	2.55	0.06	1.99	0.05	4.21	23.12
	$\lambda_{subBG}^{LED} = 690nm$	2.49	0.00	2.04	0.00	4.21	21.79
40	as-deposited	2.56		1.94		4.15	22.97
	halogen lamp	2.64	0.08	1.90	0.04	4.17	24.94
	$\lambda_{overBG}^{LED} = 405nm$	2.57	0.02	1.94	0.004	4.19	23.58
	$\lambda_{BG}^{LED} = 570nm$	2.62	0.06	1.90	0.04	4.08	23.99
	$\lambda_{subBG}^{LED} = 740nm$	2.56	0.008	1.94	0.00	4.28	23.83
50	as-deposited	2.61		1.87		4.02	23.40
	halogen lamp	2.68	0.07	1.82	0.05	3.91	24.21
	$\lambda_{overBG}^{LED} = 405nm$	2.63	0.02	1.86	0.01	4.02	23.67
	$\lambda_{BG}^{LED} = 630nm$	2.69	0.08	1.82	0.05	3.95	24.55
	$\lambda_{subBG}^{LED} = 740nm$	2.63	0.02	1.87	0.005	4.09	24.14
60	as-deposited	2.69		1.79		3.86	23.97
	halogen lamp	2.76	0.07	1.75	0.04	3.79	25.13
	$\lambda_{overBG}^{LED} = 405nm$	2.72	0.03	1.77	0.02	3.74	23.88
	$\lambda_{BG}^{LED} = 690nm$	2.75	0.06	1.74	0.05	3.65	23.93
	$\lambda_{subBG}^{LED} = 790nm$	2.72	0.03	1.78	0.01	3.86	24.61

Table 2

Change of kinetic parameters of photoinduced transformation of amorphous  $As_{40}S_{60-x}Se_x$  thin films.

$x$ , at.%	Wavenumber of LEDs peak maximum $\lambda$ , nm	$\Delta\lambda_{MAX}$ (for $d\sim 1\mu\text{m}$ )	Dispersion, $\beta$	Effective response time, $\tau$ (sec)
10	375	5.5	0.37	129
	405	11.5	0.37	101
	450	16.5	0.46	82
	525	19.5	0.84	79
	570	14.0	1.16	1412
	630	2.0	0.52	761
30	375	9.5	0.41	158
	405	10.5	0.40	88
	450	12.5	0.43	135
	525	22.5	0.61	82
	570	21	1.01	188
	630	19	1.15	673
	690	3.6	0.58	1521
50	375	5.0	0.34	104
	405	4.5	0.50	218
	450	7.5	0.52	155
	525	18.5	0.44	205
	570	21.0	0.63	198
	630	24.5	0.82	127
	690	18.5	1.12	834